

Communication

Supramolecular Sensing of a Chemical Warfare Agents Simulant by Functionalized Carbon Nanoparticles

Nunzio Tuccitto ^{1,2,*} , Luca Spitaleri ^{1,3} , Giovanni Li Destri ^{1,2} , Andrea Pappalardo ^{1,3},
Antonino Gulino ^{1,3}  and Giuseppe Trusso Sfrassetto ^{1,3,*} 

¹ Department of Chemical Sciences, University of Catania, Viale A. Doria 6, 95125 Catania, Italy; luca.spitaleri@phd.unict.it (L.S.); giolides@unict.it (G.L.D.); andrea.pappalardo@unict.it (A.P.); agulino@unict.it (A.G.)

² Laboratory for Molecular Surfaces and Nanotechnology–CSGI, Viale A. Doria 6, 95125 Catania, Italy

³ National Interuniversity Consortium for Materials Science and Technology (I.N.S.T.M.) Research Unit of Catania, Viale A. Doria 6, 95125 Catania, Italy

* Correspondence: nunzio.tuccitto@unict.it (N.T.); giuseppe.trusso@unict.it (G.T.S.);
Tel.: +39-0957385201 (G.T.S.)

Academic Editors: Alessandro D'Urso, Maria Elena Fragala and Derek J. McPhee
Received: 30 October 2020; Accepted: 2 December 2020; Published: 4 December 2020



Abstract: Real-time sensing of chemical warfare agents by optical sensors is today a crucial target to prevent terroristic attacks by chemical weapons. Here the synthesis, characterization and detection properties of a new sensor, based on covalently functionalized carbon nanoparticles, are reported. This nanosensor exploits noncovalent interactions, in particular hydrogen bonds, to detect DMMP, a simulant of nerve agents. The nanostructure of the sensor combined with the supramolecular sensing approach leads to high binding constant affinity, high selectivity and the possibility to reuse the sensor.

Keywords: carbon nanoparticles; chemical warfare agents; sensor; supramolecular recognition

1. Introduction

Chemical warfare agents (CWAs), organophosphorus compounds developed before the Second World War, are highly toxic compounds due to their ability to irreversibly inhibit the acetylcholine esterase enzyme [1].

Today, CWAs are classified into three classes: G-type, V-type and A-type (also called Novichok) (Scheme 1).

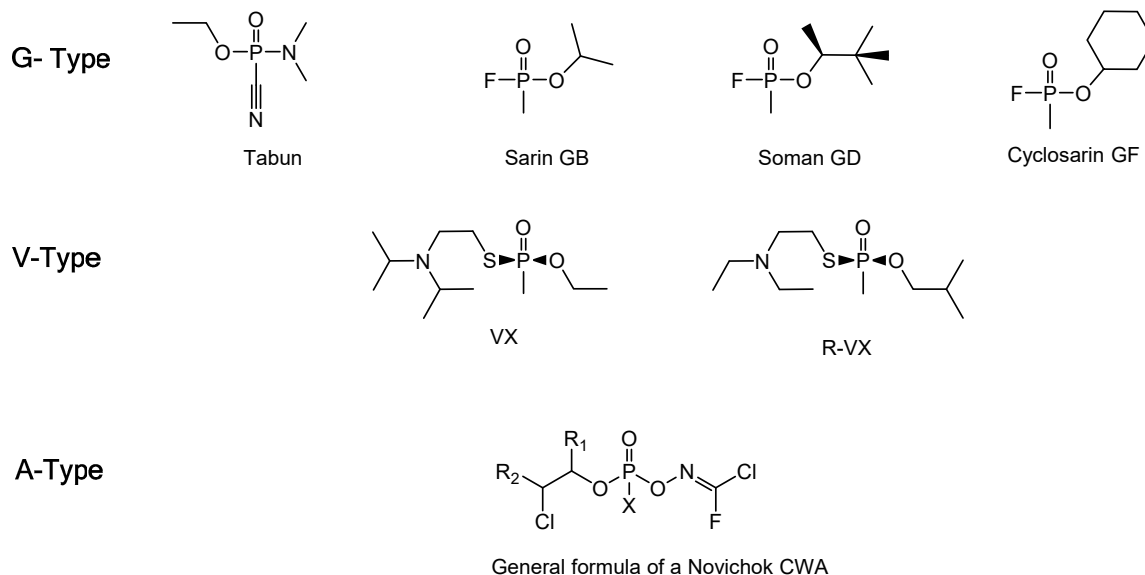
Although CWAs are today prohibited in many countries, the recent attacks in the Middle East and in Europe highlight the importance to quickly detect, in real time, the presence of these agents [2,3].

Due to the toxicity levels of G- and V-type CWAs (LC50 values of Tabun and Sarin are 2 and 1.2 ppm, respectively, while Soman and VX have LC50 of 0.9 and 0.3 ppm, respectively) [4], the ability to detect low concentration values is of primary importance.

Research activity is usually performed by using simulants, less toxic compounds having geometries and sizes very similar to real CWAs [5]. In particular, the dimethyl methylphosphonate (DMMP) is today widely recognized as one of the best simulants for G-type CWAs.

Sensing of CWAs can be performed by using two different approaches: the “covalent approach” [6], based on a covalent reaction between the sensor and the analyte that leads to a change on a specific measurable property, or the “supramolecular approach” [7], in which the analyte is recognized by exploiting noncovalent interactions with a synthetic receptor. The covalent approach shows some limits: (i) low specificity, (ii) possibility of false-positive responses and (iii) impossibility to reuse the

sensor. By contrast, the recent success of the supramolecular approach is due to the possibility to reuse the sensor, because of the formation of noncovalent interactions with the analyte [8–16], and the high efficiency (in terms of binding constant values) [17] and selectivity due to the possibility to recognize the analyte by multiple interactions (multitopic approach) [18,19].

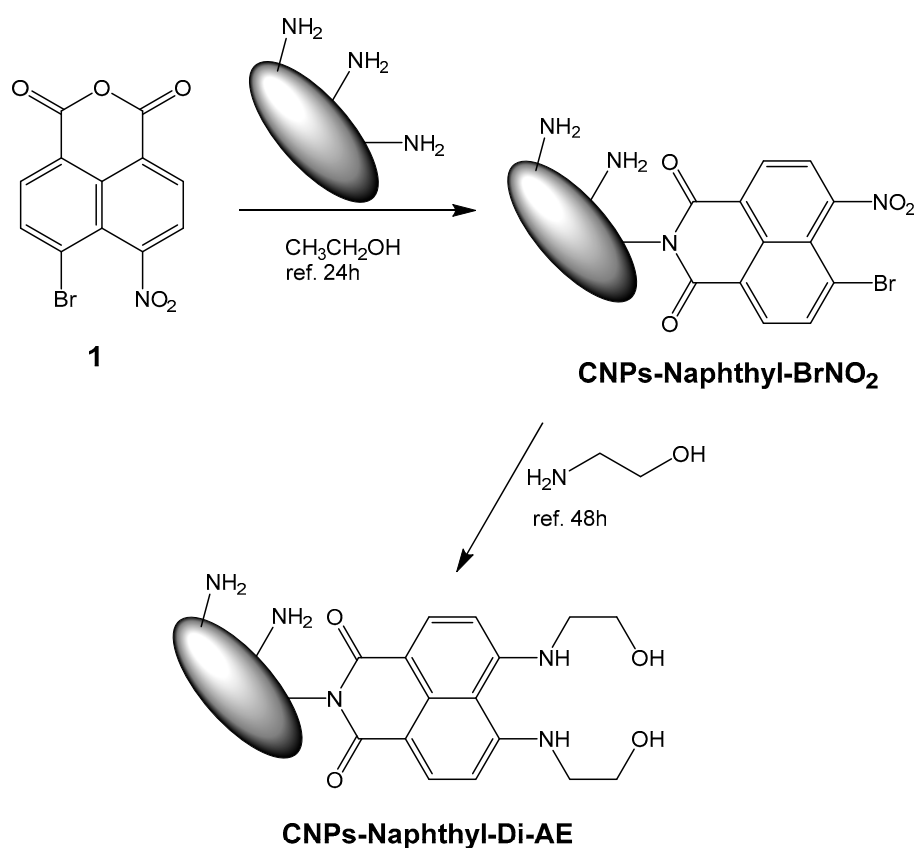


Scheme 1. Structures and names of G-type, V-type and general formula of A-type chemical warfare agents (CWAs).

Recently, we reported on the first metal-free fluorescent sensor, Naphthyl-Di-AE, able to selectively and reversibly detect DMMP via the multitopic approach by exploiting multiple hydrogen bonds [20]. Furthermore, very recently, we reported on the first nanosensor based on carbon nanoparticles (CNPs), able to detect very low concentration values of DMMP both in solution and in the gas phase [21]. The use of CNPs [22–24] for sensing purposes shows many interesting features, such as the high fluorescence quantum yield [25], water solubility, low toxicity [26], low-cost synthesis [27] and the possibility to functionalize their external shell [28].

Taking into account these considerations, here we present the implementation of the Naphthyl-Di-AE on the surface of carbon nanoparticles, leading to **CNPs-Naphthyl-Di-AE** (Scheme 2). The presence of a specific sensor for DMMP (Naphthyl-Di-AE) on the nanoparticle surface leads to the possibility to increase the selectivity towards the desired analyte target and to follow the recognition event by monitoring a specific change in the optical spectrum of the receptor.

In particular, the ethanolamine arms, responsible for hydrogen bond formation, are in the perfect geometry to recognize DMMP with both arms. With respect to our recent nanoparticle-based sensor, having the ethanolamine arms randomly bounded onto the nanoparticle surface [21], **CNPs-Naphthyl-Di-AE** show the recognition group (previously synthesized) having the optimal configuration to chelate and DMMP.



Scheme 2. Synthesis of CNPs-Naphthyl-Di-AE.

2. Results and Discussion

CNPs-Naphthyl-BrNO₂ were obtained by reacting the anhydride **1** [29] in refluxing ethanol with amino-terminal CNPs, and they were purified by centrifugation and filtration. Reaction of CNPs-Naphthyl-BrNO₂ with a large excess of ethanolamine in solvolysis leads to the CNPs-Naphthyl-Di-AE, which have been purified by centrifugation and dialysis. The ¹H-NMR spectrum suggests the covalent functionalization with the ethanolamine groups, due to the presence of aromatic signals characteristic of the naphthalic core and, in the aliphatic region, of the typical pattern of ethanolamine (see Supplementary Material).

The electronic structure of the carbon nanoparticles (CNPs) functionalized with the naphthalic probe, CNPs-Naphthyl-Di-AE, was also investigated by X-ray photoelectron spectroscopy (XPS), thus providing information on the chemical environment. XPS also gave information on the covalent anchoring of the naphthalic sensor on the CNPs surface, appropriately functionalized with –NH₂ groups. Finally, the surface elemental composition was estimated, once the relevant atomic sensitivity factors had been taken into account [30–34].

Figure 1 shows the high-resolution XPS spectrum of the CNPs-Naphthyl-Di-AE in the C 1s binding energy region. An accurate fitting of this spectrum revealed the presence of four components at 285.0, 286.0, 286.4 and 287.7 eV, respectively. The first component (285.0 eV) is due to both aliphatic and aromatic backbones [35,36]. The peaks at 286.0 eV and 286.4 eV are due to the C–N and C–OH groups, respectively [37,38]. The peak at 287.7 eV is assigned to the carbon of the amide group (–OC–NH–) [39], and the presence of this signal confirms the covalent functionalization of the CNPs with the naphthalic anhydride. Moreover, the intensity ratio between these three bands at 286.0, 286.4 and 287.7 eV is 5:2:2, and this result is in agreement with the chemical structure of the CNPs-Naphthyl-Di-AE, reported in Scheme 2. Finally, the peak at 293.2 eV is ascribed to π–π* shake-up satellites characteristic of the aromatic and conjugate systems.

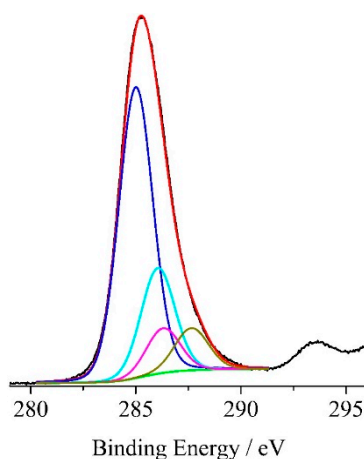


Figure 1. Al-K α excited XPS of the CNPs–naphthalic anhydride sample in the C 1s binding energy region. The blue, cyan, magenta and dark yellow lines refer to the 285.0, 286.0, 286.4 and 287.7 components; the green line refers to the background, and the red line superimposed to the experimental black profile refers to the sum of all Gaussian components.

Figure 2 shows the XPS of CNPs-Naphthyl-Di-AE in the N 1s binding energy region. The N 1s spectral profile was fitted using two Gaussian components at 400.1 and 401.7 eV. The first component (400.1 eV) is due to the nitrogen of amine groups (–NH–) [39]. The peak at 401.7 eV is due to the nitrogen of the imide group (O=C–N–C=O) [40]. The presence of O=C–N–C=O group confirms the covalent functionalization of the CNPs with the naphthalic core. The intensity ratio between the two bands at 400.1/401.7 eV is 2:1, and this result is in agreement with the chemical structure of the naphthalic anhydride molecule.

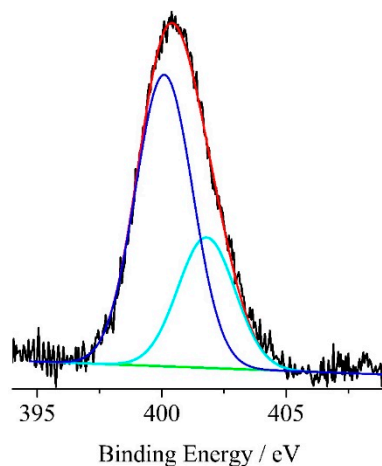


Figure 2. Al-K α excited XPS of CNPs-Naphthyl-Di-AE in the N 1s binding energy region. The blue and cyan lines refer to the 400.1 and 401.7 eV components; the green line refers to the background, and the red line superimposed to the experimental black profile refers to the sum of all Gaussian components.

Finally, Figure 3 shows the O 1s peak of the CNPs–naphthalic anhydride system. The O 1s spectral profile was fitted using four Gaussian components at 532.3, 532.9, 534.4 and 537.3 eV. The lower energy peak, located at 532.3 eV, is assigned to the –OH groups of both CNPs and naphthalic core [41]. The second peak at 532.9 eV is assigned to the imide (O=C–N–C=O) group [40,41] and further confirms the covalent functionalization of the CNPs with the naphthalic anhydride molecule. Once more, the intensity ratios of the first two peaks (2:2) presently observed are strongly in agreement with the expected intensity trend, on the basis of the structure of CNPs-Naphthyl-Di-AE. The higher energy peak located at 534.4 eV is attributed to the H₂O molecules present in the air-exposed CNPs–naphthalic

anhydride system. Besides, the 537.3 eV peak is attributed to the molecular O₂ adsorbed on the surface of the air-exposed sample [41].

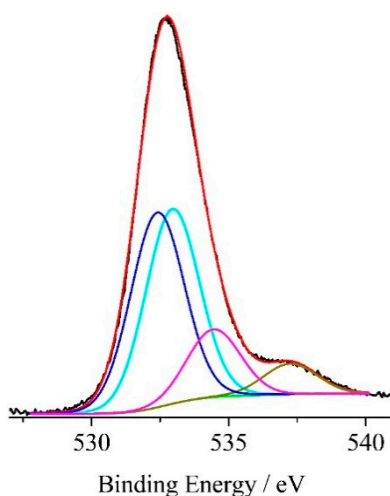


Figure 3. Al-K α excited XPS of the **CNPs-Naphthyl-Di-AE** sample in the O 1s energy region. The black line refers to the experimental profile; the green line refers to the background; the Gaussian at 532.3 (blue line), 532.9 (cyan line), 534.4 (magenta line) and 537.3 eV (dark yellow line) represent the four O 1s components; the red line, superimposed to the experimental profile, refers to the sum of the Gaussian components.

Sensing properties were evaluated by UV-Vis spectroscopy. A solution of 0.05 mg/mL of **CNPs-Naphthyl-Di-AE** in toluene shows a broad absorption band, characteristic of the carbon nanoparticles extending all over the visible and near UV region. In addition, the band relative to the Naphthyl-Di-AE sensor can be detected at 430 nm. This band was monitored during the sensing of DMMP. In particular, the progressive addition of DMMP (0–100 μ L of a 1×10^{-4} M solution in toluene) leads to a decrease of the absorbance intensity (Figure 4), in agreement with the behavior observed by using the molecular sensor in solution [20]. The nonlinear curve fit of this data indicates a binding constant affinity of $\log 5.55 \pm 0.30$, more than one order of magnitude higher with respect to that of the Naphthyl-Di-AE in solution ($\log 4.02$), thus demonstrating the higher performance of the nanosensor with respect to the molecular sensor. Notably, the calculated detection limit is 0.16 ppm (see Section 3), lower than the LC50 values of the most common CWAs used (fluorescence measurements are precluded due to the stronger emission of the carbon nanoparticle core that overlaps the emission of the naphthalic core).

Selectivity is a crucial parameter for a sensor. For this reason, we tested the UV-Vis response of **CNPs-Naphthyl-Di-AE** to different organic analytes, in order to test the efficiency of the multitopic approach. Figure 5 shows the normalized absorbance values of **CNPs-Naphthyl-Di-AE** observed upon the addition of 50 ppm of different analytes. We note that carbonyl compounds do not interact with our sensor. Organic phosphorous compounds, such as triethylphosphite, triphenylphosphine and phosphocholine cause a slight increase of the optical response. The presence of air (containing 24,000 ppm of water, 400 ppm CO₂, 5 ppm NO and 10 ppm CO), bubbled for 30 min, does not interfere with the nanosensor. On the contrary, the addition of 1 ppm of DMMP leads to a strong optical response.

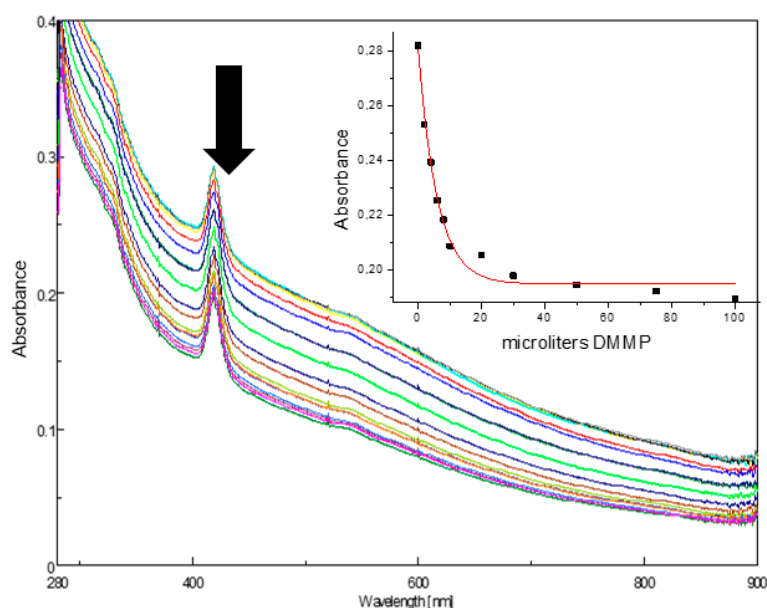


Figure 4. UV-Vis spectra of CNPs-Naphthyl-Di-AE (0.05 mg/mL in toluene) upon progressive addition of DMMP (0–100 μL of a 1×10^{-4} M solution in toluene), inset shows the calibration curve.

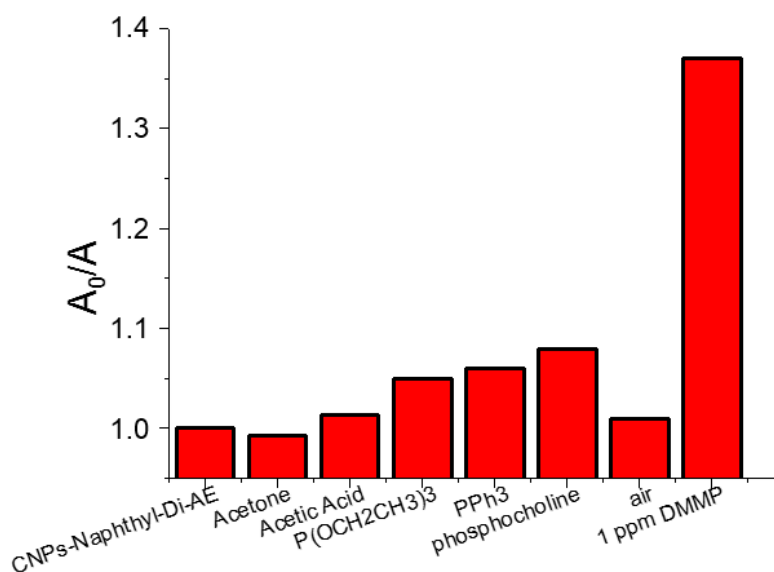


Figure 5. Normalized UV-Vis responses of CNPs-Naphthyl-Di-AE (0.05 mg/mL in toluene) to various competitive guests: 50 ppm of acetone, acetic acid, triethylphosphite ($\text{P}(\text{OCH}_2\text{CH}_3)_3$), triphenylphosphine (PPh_3) and phosphocholine; air (bubbled for 30 min); and DMMP (1 ppm). Bars represent the initial over the final absorbance values at 430 nm.

3. Materials and Methods

3.1. General Experimental Methods

The NMR experiments were carried out at 27°C on a Varian UNITY Inova 500 MHz spectrometer (^1H at 499.88 MHz, ^{13}C -NMR at 125.7 MHz, Varian-Agilent, Santa Clara, CA, USA) equipped with a pulse-field gradient module (Z axis) and a tunable 5 mm Varian inverse detection probe (ID-PFG). UV-Vis measurements were carried out using a JASCO V-630 spectrophotometer (Mettler Toledo, Novate Milanese, Italy) at room temperature. All chemicals were reagent grade (Sigma Aldrich, Buchs, Switzerland) and used without further purification. X-ray photoelectron spectra (XPS) were

measured at a 45° take-off angle relative to the surface normal with a PHI 5600 Multi Technique System (Physical Electronics GmbH, Feldkirchen, Germany, base pressure of the main chamber 3×10^{-8} Pa) [35,36]. Samples were excited with the Al-K α X-ray radiation using a pass energy of 5.85 eV. Structures due to the K α satellite radiations were subtracted from the spectra prior to data processing. Spectra calibration was achieved by fixing the Ag 3d5/2 peak of a clean sample at 368.3 eV; this method turned the C 1s main peak at 285.0 eV [35,36,42]. The instrumental energy resolution was ≤ 0.5 eV. The XPS peak intensities were obtained after Shirley background removal [35,36]. The atomic concentration analysis was performed by taking into account the relevant atomic sensitivity factors. The fittings of the C 1s, N 1s and O 1s XP spectra were carried out using Gaussian envelopes after subtraction of the background until there was the highest possible correlation between the experimental spectrum and the theoretical profile. The residual or agreement factor R , defined by $R = [\sum(F_{\text{obs}} - F_{\text{calc}})^2 / \sum(F_{\text{obs}})^2]^{1/2}$, after minimization of the function $\sum(F_{\text{obs}} - F_{\text{calc}})^2$, converged to the value of 0.03. The fitting was performed using the XPSPEAK4.1 software (free, fully featured, software for the analysis of XPS spectra written by Raymund Kwok). Samples for XPS measurement were deposited on silicon substrates.

3.2. Synthesis of CNPs-Naphthyl-BrNO₂

One hundred milligrams of amino-terminal CNPs [43] was dissolved in 15 mL of absolute ethanol, and 70 mg (0.217 mmol) of **1** was added. The mixture was stirred at reflux for 24 h under nitrogen atmosphere. Solvent was removed by rotavapor, and the **CNPs-Naphthyl-BrNO₂** were purified by centrifugation and filtration in hot ethanol.

3.3. Synthesis of CNPs-Naphthyl-Di-AE

Twenty milligrams of **CNPs-Naphthyl-BrNO₂** was dissolved in 10 mL of ethanolamine, and the mixture was refluxed under nitrogen atmosphere for 48 h. The excess of ethanolamine was removed under reduced pressure, and the **CNPs-Naphthyl-Di-AE** were purified by centrifugation and dialysis.

3.4. Procedure for UV-Vis Titrations

From a guest stock solution (1.0×10^{-4} M) in toluene, different volumes (0, 2, 4, 6, 8, 10, 20, 30, 50, 75, 100 μ L) were added to the host (0.05 mg/mL in toluene), and the UV-Vis spectra were recorded at 25 °C. The apparent binding affinities of **CNPs-Naphthyl-Di-AE** with DMMP were estimated by using HypSpec (version 1.1.33) [44–46], a software designed to extract equilibrium constants from potentiometric and/or spectrophotometric titration data. HypSpec starts with an assumed complex formation scheme and uses a least-squares approach to derive the spectra of the complexes and the stability constants. χ^2 test (chi-square) was applied, where the residuals followed a normal distribution (for a distribution approximately normal, the χ^2 test value is around 12 or less). In all of the cases, $\chi^2 \leq 10$ was found, as obtained by 3 independent measurement sets. Limit of detection was calculated by the method of the calibration curve using the formula $DL = 3s/K$, where s is the standard deviation of the blank and K is the slope of the calibration curve.

4. Conclusions

In the present study, we report the covalent functionalization of carbon nanoparticles by a selective sensor of Chemical Warfare Agents. The presence of a specific sensor for DMMP (Naphthyl-Di-AE) on the carbon nanoparticle surface leads to the possibility to increase the selectivity towards the given analyte target and to follow the recognition event by monitoring a specific change of the optic spectrum of the receptor. The new nanosensor shows high binding affinity towards DMMP, high selectivity and a sub-ppm detection limit. The possibility to tune the molecular structure of the external shell of the carbon nanoparticles leads to a wide range of applications, including sensing applications. Studies are ongoing to obtain functionalized fluorescent carbon nanoparticles suitable for real prototypes to be commonly used.

Supplementary Materials: The following are available online. Figure S1: ¹H-NMR spectrum of CNPs-Naphthyl-Di-AE in DMSO-*d*₆; Figure S2: UV-Vis titration between CNPs-Naphthyl-Di-AE and DMMP.

Author Contributions: Conceptualization, N.T. and G.T.S.; XPS analysis, L.S. and A.G.; synthesis, A.P. and G.T.S.; validation, G.L.D.; writing—original draft preparation, N.T. and G.T.S. All authors have read and agreed to the published version of the manuscript.

Funding: This research was funded by the University of Catania (PIA.CE.RI 2020-2022–Linea Intervento 2).

Acknowledgments: The authors thank the project “Nati4Smart” University of Catania for financial support.

Conflicts of Interest: The authors declare no conflict of interest.

References

1. Zammataro, A.; Santonocito, R.; Pappalardo, A.; Trusso Sfrazzetto, G. Catalytic Degradation of Nerve Agents. *Catalysts* **2020**, *10*, 881. [[CrossRef](#)]
2. Stone, R.U.K. attack puts nerve agent in the spotlight. *Science* **2018**, *359*, 1314–1315. [[CrossRef](#)] [[PubMed](#)]
3. Stone, R. How to defeat a nerve agent. *Science* **2018**, *359*, 23. [[CrossRef](#)] [[PubMed](#)]
4. Wiener, S.W.; Hoffman, R.S. Nerve Agents: A Comprehensive Review. *J. Intensive. Care Med.* **2004**, *19*, 22–37. [[CrossRef](#)] [[PubMed](#)]
5. Lavoie, J.; Srinivasan, S.; Nagarajan, R. Using cheminformatics to find simulants for chemical warfare agents. *J. Hazard. Mater.* **2011**, *194*, 85–91. [[CrossRef](#)] [[PubMed](#)]
6. Jang, Y.J.; Kim, K.; Tsay, O.G.; Atwood, D.A.; Churchill, D.G. Update 1 of: Destruction and detection of Chemical Warfare Agents. *Chem. Rev.* **2015**, *115*, PR1–PR76. [[CrossRef](#)]
7. Sambrook, M.R.; Notman, S. Supramolecular chemistry and chemical warfare agents: From fundamentals of recognition to catalysis and sensing. *Chem. Soc. Rev.* **2013**, *42*, 9251–9267. [[CrossRef](#)]
8. Hiscock, J.R.; Piana, F.; Sambrook, M.R.; Wells, N.J.; Clark, A.J.; Vincent, J.C.; Busschaert, N.; Brown, R.C.D.; Gale, P.A. Detection of nerve agent via perturbation of supramolecular gel formation. *Chem. Commun.* **2013**, *49*, 9119–9121. [[CrossRef](#)]
9. Sambrook, M.R.; Hiscock, J.R.; Cook, A.; Green, A.C.; Holden, I.; Vincent, J.C.; Gale, P.A. Hydrogen bond-mediated recognition of the chemical warfare agent soman (GD). *Chem. Commun.* **2012**, *48*, 5605–5607. [[CrossRef](#)]
10. Chen, S.; Ruan, Y.; Brown, J.D.; Gallucci, J.; Maslak, V.; Hadad, C.M.; Badjic, J.D. Assembly of Amphiphilic Baskets into Stimuli-Responsive Vesicles. Developing a Strategy for the Detection of Organophosphorus Chemical Nerve Agents. *J. Am. Chem. Soc.* **2013**, *135*, 14964–14967. [[CrossRef](#)]
11. Ruan, Y.; Dalkilic, E.; Peterson, P.W.; Pandit, A.; Dastan, A.; Brown, J.D.; Polen, S.M.; Hadad, C.M.; Badjic, J.D. Trapping of Organophosphorus Chemical Nerve Agents in Water with Amino Acid Functionalized Baskets. *Chem. Eur. J.* **2014**, *20*, 4251–4256. [[CrossRef](#)]
12. Chen, S.; Ruan, Y.; Brown, J.D.; Hadad, C.M.; Badjic, J.D. Recognition Characteristics of an Adaptive Vesicular Assembly of Amphiphilic Baskets for Selective Detection and Mitigation of Toxic Nerve Agents. *J. Am. Chem. Soc.* **2014**, *136*, 17337–17342. [[CrossRef](#)] [[PubMed](#)]
13. Ruan, Y.; Chen, S.; Brown, J.D.; Hadad, C.M.; Badjic, J.D. Ubiquitous Assembly of Amphiphilic Baskets into Unilamellar Vesicles and Their Recognition Characteristics. *Org. Lett.* **2015**, *17*, 852–855. [[CrossRef](#)] [[PubMed](#)]
14. Pappalardo, A.; Amato, M.E.; Ballistreri, F.P.; La Paglia Fragola, V.; Tomaselli, G.A.; Toscano, R.M.; Trusso Sfrazzetto, G. Binding of Reactive Organophosphate by Oximes via Hydrogen Bond. *J. Chem. Sci.* **2013**, *125*, 869–873. [[CrossRef](#)]
15. Gulino, A.; Trusso Sfrazzetto, G.; Millesi, S.; Pappalardo, A.; Tomaselli, G.A.; Ballistreri, F.P.; Toscano, R.M.; Fragalà, L. Nerve Gas Simulant Sensing by an Uranyl-Salen Monolayer Covalently Anchored on Quartz Substrates. *Chem. Eur. J.* **2017**, *23*, 1576–1583.
16. Puglisi, R.; Mineo, P.G.; Pappalardo, A.; Gulino, A.; Trusso Sfrazzetto, G. Supramolecular Detection of a Nerve Agent Simulant by Fluorescent Zn–Salen Oligomer Receptors. *Molecules* **2019**, *24*, 2160. [[CrossRef](#)]
17. Barba-Bon, A.; Costero, A.M.; Parra, M.; Gil, S.; Martinez-Manez, R.; Sancenon, F.; Gale, P.A.; Hiscock, J.R. Neutral 1,3-Diindolylureas for Nerve Agent Remediation. *Chem. Eur. J.* **2013**, *19*, 1586–1590. [[CrossRef](#)]
18. Puglisi, R.; Pappalardo, A.; Gulino, A.; Trusso Sfrazzetto, G. Supramolecular recognition of CWAs simulant by metal-salen complexes: The first multi-topic approach. *Chem. Commun.* **2018**, *54*, 11156–11159. [[CrossRef](#)]

19. Legnani, L.; Puglisi, R.; Pappalardo, A.; Chiacchio, M.A. Trusso Sfrazzetto, G. Supramolecular recognition of phosphocholine by an enzyme-like cavitand receptor. *Chem. Commun.* **2020**, *56*, 539–542. [[CrossRef](#)]
20. Puglisi, R.; Pappalardo, A.; Gulino, A.; Trusso Sfrazzetto, G. Multitopic Supramolecular Detection of Chemical Warfare Agents by Fluorescent Sensors. *ACS Omega* **2019**, *4*, 7550–7555. [[CrossRef](#)]
21. Tuccitto, N.; Riela, L.; Zammataro, A.; Spitaleri, L.; Li-Destri, G.; Sfuncia, G.; Nicotra, G.; Capizzi, G.; Trusso Sfrazzetto, G. Functionalized Carbon Nanoparticle-Based Sensors for Chemical Warfare Agents. *ACS Appl. Nano Mater.* **2020**, *3*, 8182–8191. [[CrossRef](#)]
22. Tuccitto, N.; Li-Destri, G.; Messina, G.M.L.; Marletta, G. Fluorescent quantum dots make feasible long-range transmission of molecular bits. *J. Phys. Chem. Lett.* **2017**, *8*, 3861–3866. [[CrossRef](#)] [[PubMed](#)]
23. Li-Destri, G.; Fichera, L.; Zammataro, A.; Trusso Sfrazzetto, G.; Tuccitto, N. Self-assembled carbon nanoparticles as messengers for artificial chemical communication. *Nanoscale* **2019**, *11*, 14203–14209. [[CrossRef](#)] [[PubMed](#)]
24. Fichera, L.; Li-Destri, G.; Tuccitto, N. Fluorescent nanoparticle-based Internet of things. *Nanoscale* **2020**, *12*, 9817–9823. [[CrossRef](#)] [[PubMed](#)]
25. Qu, S.N.; Chen, H.; Zheng, X.M.; Cao, J.S.; Liu, W.Y. Ratiometric fluorescent nanosensor based on water soluble carbon nanodots with multiple sensing capacities. *Nanoscale* **2013**, *5*, 5514–5518. [[CrossRef](#)]
26. Zhu, A.W.; Qu, Q.; Shao, X.L.; Kong, B.; Tian, Y. Carbon-Dot-Based Dual-Emission Nanohybrid Produces a Ratiometric Fluorescent Sensor for In Vivo Imaging of Cellular Copper Ions. *Angew. Chem. Int. Ed.* **2012**, *51*, 7185–7189. [[CrossRef](#)]
27. Baptista, F.R.; Belhout, S.A.; Giordani, S.; Quinn, S.J. Recent developments in carbon nanomaterial sensors. *Chem. Soc. Rev.* **2015**, *44*, 4433–4453. [[CrossRef](#)]
28. Zammataro, A.; Gangemi, C.M.A.; Pappalardo, A.; Toscano, R.M.; Puglisi, R.; Nicotra, G.; Fragalà, M.E.; Tuccitto, N.; Trusso Sfrazzetto, G. Covalently functionalized carbon nanoparticles with a chiral Mn-Salen: A new nanocatalyst for enantioselective epoxidation of alkenes. *Chem. Commun.* **2019**, *55*, 5255–5258. [[CrossRef](#)]
29. Giuffrida, M.L.; Trusso Sfrazzetto, G.; Satriano, C.; Zimbone, S.; Tomaselli, G.A.; Copani, A.; Rizzarelli, E. A New Ratiometric Lysosomal Copper(II) Fluorescent Probe to Map a Dynamic Metallome in Live Cells. *Inorg. Chem.* **2018**, *57*, 2365–2368. [[CrossRef](#)]
30. Spitaleri, L.; Gangemi, C.M.A.; Purrello, R.; Nicotra, G.; Trusso Sfrazzetto, G.; Casella, G.; Casarin, M.; Gulino, A. Covalently Conjugated Gold–Porphyrin Nanostructures. *Nanomaterials* **2020**, *10*, 1644. [[CrossRef](#)]
31. Gulino, A.; Gupta, T.; Mineo, P.G.; van der Boom, M.E. Selective NO_x optical sensing with surface-confined osmium polypyridyl complexes. *Chem. Commun.* **2007**, 4878–4880. [[CrossRef](#)] [[PubMed](#)]
32. Contino, A.; Maccarrone, G.; Fragalà, M.E.; Spitaleri, L.; Gulino, A. Gold–Porphyrin Monolayers Assembled on Inorganic Surfaces. *Chem. Eur. J.* **2017**, *23*, 14937–14943. [[CrossRef](#)] [[PubMed](#)]
33. Contino, A.; Maccarrone, G.; Spitaleri, L.; Torrisi, L.; Nicotra, G.; Gulino, A. One Pot Synthesis of Au₂ZnO Core-Shell Nanoparticles Using a Zn Complex Acting as ZnO Precursor, Capping and Reducing Agent During the Formation of Au NPs. *Eur. J. Inorg. Chem.* **2018**, *43*, 4678–4683. [[CrossRef](#)]
34. Spitaleri, L.; Nicotra, G.; Zimbone, M.; Contino, A.; Maccarrone, G.; Alberti, A.; Gulino, A. Fast and Efficient Sun Light Photocatalytic Activity of Au₂ZnO Core–Shell Nanoparticles Prepared by a One-Pot Synthesis. *ACS Omega* **2019**, *4*, 15061–15066. [[CrossRef](#)] [[PubMed](#)]
35. Briggs, D.; Grant, J.T. *Surface Analysis by Auger and X-ray Photoelectron Spectroscopy*; IM Publications: Chichester, UK; Surface Spectra Ltd.: Manchester, UK, 2003.
36. Gulino, A. Structural and electronic characterization of self-assembled molecular nanoarchitectures by X-ray photoelectron spectroscopy. *Anal. Bioanal. Chem.* **2013**, *405*, 1479–1495. [[CrossRef](#)] [[PubMed](#)]
37. Schneider, J.; Reckmeier, C.J.; Xiong, Y.; von Seckendorff, M.; Susha, A.S.; Kasák, P.; Rogach, A.L. Molecular Fluorescence in Citric Acid-Based Carbon Dots. *J. Phys. Chem. C* **2017**, *121*, 2014–2022. [[CrossRef](#)]
38. Graf, N.; Yegen, E.; Gross, T.; Lippi, A.; Weigel, W.; Krakert, S.; Terfort, A.; Unger, W.E.S. XPS and NEXAFS studies of aliphatic and aromatic amine species on functionalized surfaces. *Surf. Sci.* **2009**, *603*, 2849–2860. [[CrossRef](#)]
39. Liu, Y.; Yu, Z.-L.; Zhang, Y.-M.; Guo, D.-S.; Liu, Y.-P. Supramolecular Architectures of β -Cyclodextrin-Modified Chitosan and Pyrene Derivatives Mediated by Carbon Nanotubes and Their DNA Condensation. *J. Am. Chem. Soc.* **2008**, *130*, 10431–10439. [[CrossRef](#)]

40. Chenite, A.; Selmani, A. Cr/phthalimide system: XPS study of interfacial reactions. *Surf. Sci.* **1994**, *301*, 197–202. [[CrossRef](#)]
41. Parvizi, R.; Azad, S.; Dashtian, K.; Ghaedi, M.; Heidari, H. Natural Source-Based Graphene as Sensitising Agents for Air Quality Monitoring. *Sci. Rep.* **2019**, *9*, 3798. [[CrossRef](#)]
42. Greczynski, G.; Hultman, L. Compromising science by ignorant instrument calibration—Need to revisit half a century of published XPS data. *Angew. Chem. Int. Ed.* **2020**. [[CrossRef](#)]
43. Fichera, L.; Li-Destri, G.; Ruffino, R.; Messina, G.M.L.; Tuccitto, N. Reactive nanomessengers for artificial chemical communication. *Phys. Chem. Chem. Phys.* **2019**, *21*, 16223–16229. [[CrossRef](#)] [[PubMed](#)]
44. Pappalardo, A.; Amato, M.E.; Ballistreri, F.P.; Tomaselli, G.A.; Toscano, R.M.; Trusso Sfrazzetto, G. Pair of Diastereomeric Uranyl Salen Cavitands Displaying Opposite Enantiodiscrimination of α -Amino Acid Ammonium Salts. *J. Org. Chem.* **2012**, *77*, 7684–7687. [[CrossRef](#)] [[PubMed](#)]
45. Puglisi, R.; Ballistreri, F.P.; Gangemi, C.M.A.; Toscano, R.M.; Tomaselli, G.A.; Pappalardo, A.; Trusso Sfrazzetto, G. Chiral Zn–salen complexes: A new class of fluorescent receptors for enantiodiscrimination of chiral amines. *New J. Chem.* **2017**, *41*, 911–915. [[CrossRef](#)]
46. Gans, P.; Sabatini, A.; Vacca, A. Investigation of equilibria in solution. Determination of equilibrium constants with the HYPERQUAD suite of programs. *Talanta* **1996**, *43*, 1739–1753. [[CrossRef](#)]

Sample Availability: Samples of the compounds are available from the authors.

Publisher’s Note: MDPI stays neutral with regard to jurisdictional claims in published maps and institutional affiliations.



© 2020 by the authors. Licensee MDPI, Basel, Switzerland. This article is an open access article distributed under the terms and conditions of the Creative Commons Attribution (CC BY) license (<http://creativecommons.org/licenses/by/4.0/>).